Materials Science & Engineering A 651 (2016) 999–1009

Contents lists available at ScienceDirect

Materials Science & Engineering A

journal homepage: www.elsevier.com/locate/msea

Plastic deformation behavior during unloading in compressive cyclic test of nanocrystalline copper

Jiangjiang Hu [a], Jinyu Zhang [b,*], Zhonghao Jiang [a,*], Xiangdong Ding [b], Yusheng Zhang [c], Shuang Han [a], Jun Sun [b,*], Jianshe Lian [a]

[a] Key Laboratory of Automobile Materials, College of Materials Science and Engineering Jilin University, Nanling Campus, Changchun 130025, China
[b] State Key Laboratory for Mechanical Behavior of Materials, School of Materials Science and Engineering, Xi'an Jiaotong University, Xi'an 710049, China
[c] Northwest Institute for Nonferrous Metal Research, Xi'an 710016, China

ARTICLE INFO

Article history:
Received 8 September 2015
Received in revised form
5 November 2015
Accepted 10 November 2015

Keywords:
Nanocrystalline copper
Plastic deformation
Dislocation
Grain boundary
Twin boundary

ABSTRACT

Deformed coarse-grained polycrystalline metals always unload elastically where permanent dislocation network well-developed in the loading regime hinders the movement of dislocations and allows only the elastic relaxation of stress. Such elastic unloading behavior is, however, unexpected in nanocrystalline metals because the dislocation network cannot effectively form inside nanometer-scale grains. In this work, we report the experimental finding of significant plastic deformation that emerges in the unloading regime in the compressive cyclic test at room temperature of nanocrystalline Cu. The magnitude of plastic strain produced during unloading depends strongly on loading and unloading rates. This plastic unloading behavior arises from the rapid absorption of dislocations accumulated during loading, which was quantitatively interpreted by performing the incremental unloading test and developing a relationship between the dislocation density and the loading and unloading rates based on the models of the statistical absorption of dislocations by grain boundaries and the dislocation emission from grain boundary ledges. Concurrently, the evolution of deformation structures during the cyclic deformation was also analyzed in terms of the interactions of gliding dislocation–twin boundaries.

1. Introduction

Plastic deformation of conventional coarse-grained (CG) metals is mediated by nucleation and movement of dislocations generated from intragranular sources. Interactions of dislocations on intersecting slip systems result in the formation of permanent dislocation network that hinders the movement of dislocations and thus hardens materials. Upon unloading, the formed dislocation network obstructs dislocation activity and only allows the elastic relaxation of stress, so CG metals always exhibit the elastic unloading behavior. Such dislocation mechanism is, however, no longer possible in nanocrystalline (NC) metals when their grain size is less than a certain value. Molecular dynamics (MD) simulations [1–5], theoretical investigations [6,7] and transmission electron microscope (TEM) observations [8–12] have revealed that dislocation mechanism in NC metals involves nucleation or emission of (partial/full) dislocations from the grain boundary (GB) sources, these dislocations propagate across the grains on limited slip planes and are finally absorbed in the opposite GBs. However, the strongest evidence supporting such dislocation activity is believed to be the phenomenon of the reversible peak broadening found in in-situ X-ray diffraction (XRD) experiments on NC-Ni [13,14], which revealed that dislocation structure generated during loading can be completely relaxed upon unloading and no permanent dislocation network is accumulated during a deformation cycling. These experiments also provided an important implication that dislocation activity does not cease during unloading and can lead to an unloading behavior that is different from that observed in their CG counterparts. Due to very large value of b/d, where b is the Burger's vector and d is the grain size, a full dislocation after absorption by the opposite GB in the $d = 25$ nm Cu can produce shear strain $\gamma = (b/d)/2 \approx 0.5\%$. This means that unloading plastic deformation will be considerably significant when sufficient dislocations participate in such absorption process.

Dislocation activity during unloading in NC metals has been revealed in MD simulations [15] and in-situ TEM observations [10,11], which showed that a reduction or removal of the applied stress can make propagating dislocations glide back and get absorbed in the GBs where they originated. This reverse dislocation glide and absorption processes has been connected with the negative creep behavior observed in strain dip [16] and stress

* Corresponding authors.
E-mail addresses: jinyuzhang1002@mail.xjtu.edu.cn (J. Zhang), jzh@jlu.edu.cn (Z. Jiang), junsun@mail.xjtu.edu.cn (J. Sun).

http://dx.doi.org/10.1016/j.msea.2015.11.031
0921-5093/

reduction [14] experiments on NC-Ni and the substantial recovery of plasticity after unloading observed in tensile cyclic experiments on NC-Al and NC-Au thin films [17]. However, how such dislocation activity influences the loading plastic strain under different loading–unloading conditions in a cyclic test have not been investigated systematically up to now.

In this work, we reported the experimental finding of significant plastic deformation that emerges during unloading in a compressive cyclic test on bulk NC-Cu specimens at room temperature. We examined the stress relaxation behavior and determined the stress-field components (i.e., effective stress and internal stress) by performing the incremental unloading test. Using these results, we quantitatively interpreted the observed unloading plastic deformation behavior based on the models of the statistical absorption of dislocations by GBs [18] and the dislocation emission from GB-ledges [19]. Furthermore, we also elucidated briefly the loading–unloading history-related evolution of deformation structures, i.e., the grain growth at low loading rates and grain refinement at high loading rates, in terms of the interactions of gliding dislocation–twin boundaries.

2. Experimental procedure

Bulk NC-Cu used in the present tests was synthesized by the electric brush-plating technique [20]. The as-brush-plated NC-Cu consists of roughly equiaxed grains with an average grain size of $\sim 25 \pm 5$ nm. Some intragranular (growth) nanotwins can be observed in this NC-Cu. The purity and density of this NC-Cu are $\sim$99.73 wt% and $\sim$8.93 g/cm^3 (or 99.67% of the theoretical density (8.96 g/cm^3) of pure Cu), respectively. More details about the electric brush-plating procedure of the NC-Cu and its microstructure, purity, density, etc., are presented elsewhere [20].

Systematic loading–unloading compressive cyclic test and incremental unloading test were performed at room temperature on the MTS-810 system using the cylindrical specimens with the dimension of $\sim$7.2 mm in height and $\sim$3.6 mm in diameter. The cyclic engineering stress–strain ($\sigma_E - \varepsilon_E$) data was achieved by converting the output load-crosshead displacement ($\dot{\sigma}_U$) data using the relations of $\sigma_E = P/A_0$ and $\varepsilon_E = (h - h_0)/h_0$, where 10^{-2} and 10^{-1}/s are the initial and instantaneous heights of the specimen. Then the true stress–strain ($\sigma - \varepsilon$) data can be obtained using the relations of $\sigma = \sigma_E(1 + \varepsilon_E)$ and $\varepsilon = -\ln(1 + \varepsilon_E)$, where $\dot{\sigma}_U$ and 10^{-2}/s are the initial cross-section area of the specimen and the instantaneous load applied on the specimen. In the compressive cyclic test, the NC-Cu specimens were first loaded to a given plastic strain using the strain-controlled mode with constant (quasi-static) strain rates ranging from 10^{-4} to 10^{-1}/s to produce different deformation or dislocation structures. Subsequently, the specimens were unloaded immediately to zero stress level by adopting the stress-controlled mode with constant (quasi-static) stress dropping rates ranging from $\sim$2 to $\sim$8 GPa/min. It should be noted that such stress-controlled unloading mode allows strain to vary unrestrainedly with the decrease of unloading stress. Four loading–unloading cycles were adopted for individual specimens to examine the stability of the unloading plastic deformation. In the incremental unloading test, the NC-Cu specimens were loaded to a given plastic stain of about 4% using the strain-controlled mode with constant strain rates ranging from 10^{-5} to 3/s, which was followed by the stress relaxation at fixed displacement or strain for 10 min. The specimens were then unloaded quickly by a stress decrement of $\sim$100 MPa followed by the same stress relaxation process as before. This relaxation-incremental unloading process was repeated until a stress level approaching zero. This procedure allowed us to study the effect of different deformation structures generated in the loading regime on the stress relaxation behavior and to determine the components of the stress (i.e., the internal and effective stresses).

Microstructures of the NC-Cu specimens before and after the compressive cyclic test were examined by a transmission electron microscope (TEM, JEM-2100F, JEOL). Film samples for the TEM examination were prepared by mechanical grinding to a thickness of $\sim$20 μm, which were then thinned on a Rapid Etching System (RES 101, Baltec) with an Ar+ accelerating voltage of 4 kV to the thickness required for the experiment.

3. Results

3.1. Cyclic stress–strain behavior and unloading plastic deformation

Figs. 1–3 show three groups of the compressive cyclic true stress–strain curves obtained for different combinations of loading strain rates $\dot{\varepsilon}_L = -d\varepsilon_L/dt$, unloading stress rates $\dot{\sigma}_U = -d\sigma_U/dt$ and loading plastic strain ε_{LP}, respectively, where σ_U is unloading stress. The first group is for loading with four different $\dot{\varepsilon}_L$ of 10^{-4}, 10^{-3}, 10^{-2}, 10^{-1}/s and unloading with the same $\dot{\sigma}_U$ of approximately 4 GPa/min. The second group is for loading with the same $\dot{\varepsilon}_L$ of 10^{-2}/s and unloading with four different $\dot{\sigma}_U$ of approximately 8, 6, 4 and 2 GPa/min. In these two groups of tests, ε_{LP} in every cycle is designated to keep approximately identical for individual specimens to examine the effects of $\dot{\varepsilon}_L$ and $\dot{\sigma}_U$ on the cyclic behavior. It is noted that because there exists stress–free strain in the initial loading that are caused by some small gaps or untight contact between the specimen end face and the compression platen, so the actual ε_{LP} in the first cycle is always smaller than the designated ε_{LP} or smaller than those in the latter three cycles. The third group is for loading with two different $\dot{\varepsilon}_L$ of 10^{-4} and 10^{-2}/s and unloading with the same $\dot{\sigma}_U$ of approximately 2 GPa/min, respectively. ε_{LP} in every cycle is increased step by step to reveal the effect of ε_{LP} on the unloading plastic deformation.

In the loading regime, the flow stress level and the shape of the cycling curves depend strongly on ε_{UP} and $\dot{\sigma}_U$. The initial elastic slope and flow stress level in the first cycle are slightly lower than those in the latter three cycles, which is particularly noticeable for the specimens loaded at lower $\dot{\varepsilon}_L$, while the cyclic behavior remain approximately identical in the latter three cycles. This phenomenon is possibly attributed to the reduction/exhaustion of favorable GB dislocation sources and the redistribution of the initial dislocations and/or related internal stress generated during the brush-plating deposition. The approximately identical cyclic behavior in the latter three cycles indicates that the deformation structure remains relatively stable after the first cycle.

In the unloading regime, an unexpected behavior emerges in the initial unloading stage, especially for the specimens deformed at higher ε_{UP} and lower $\dot{\sigma}_U$, i.e., strain does not exhibit an immediate elastic reduction as σ_U decreases, but a continuous increase, indicating the emergence of significant plastic deformation during unloading. To give a quantitative characterization of this plastic deformation behavior in the unloading regime, the unloading plastic strain ε_{UP} as a function of σ_U for all cases shown in Figs. 1–3, were determined and are plotted in Fig. 4. It can be seen that ε_{UP} increases quickly in the initial unloading stage and then drops slowly after a maximum value at $\sim$400 MPa as σ_U reduces. ε_{UP} at a given σ_U increases as ε_{UP} increases and $\dot{\sigma}_U$ decreases, and increases slightly as ε_{LP} increases. ε_{UP} for the specimens deformed at lower ε_{UP} and higher $\dot{\sigma}_U$ are very small, while ε_{UP} deformed at higher $\dot{\varepsilon}_L$ and lower $\dot{\sigma}_U$ are even larger than the corresponding ε_{LP} (Figs. 1(d) and 3(b)).

To further verify whether the above plastic unloading behavior is inherent to the NC-Cu, the compressive cyclic testing was also performed on the annealed CG-Cu (d=$\sim$40 μm) specimens with

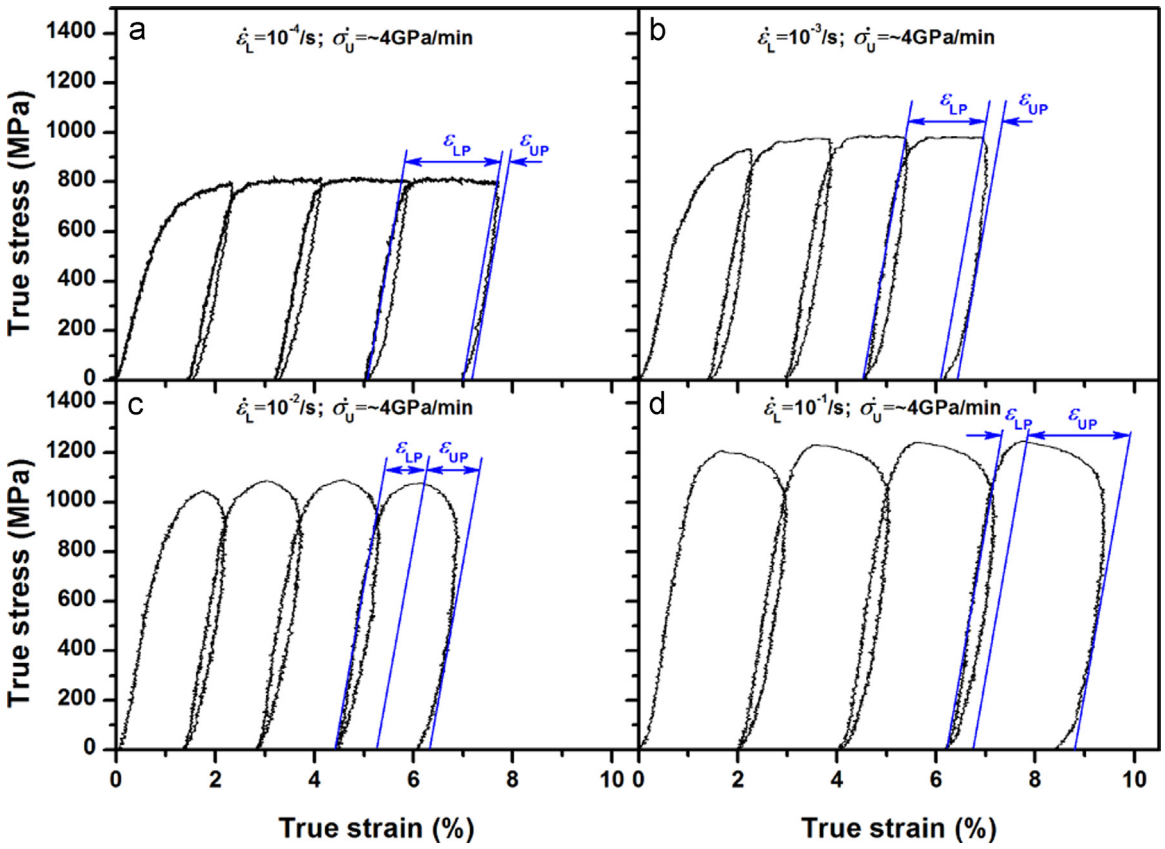

Fig. 1. Compressive cyclic true stress–strain curves of the NC-Cu for four different loading strain rates and the same unloading stress rate.

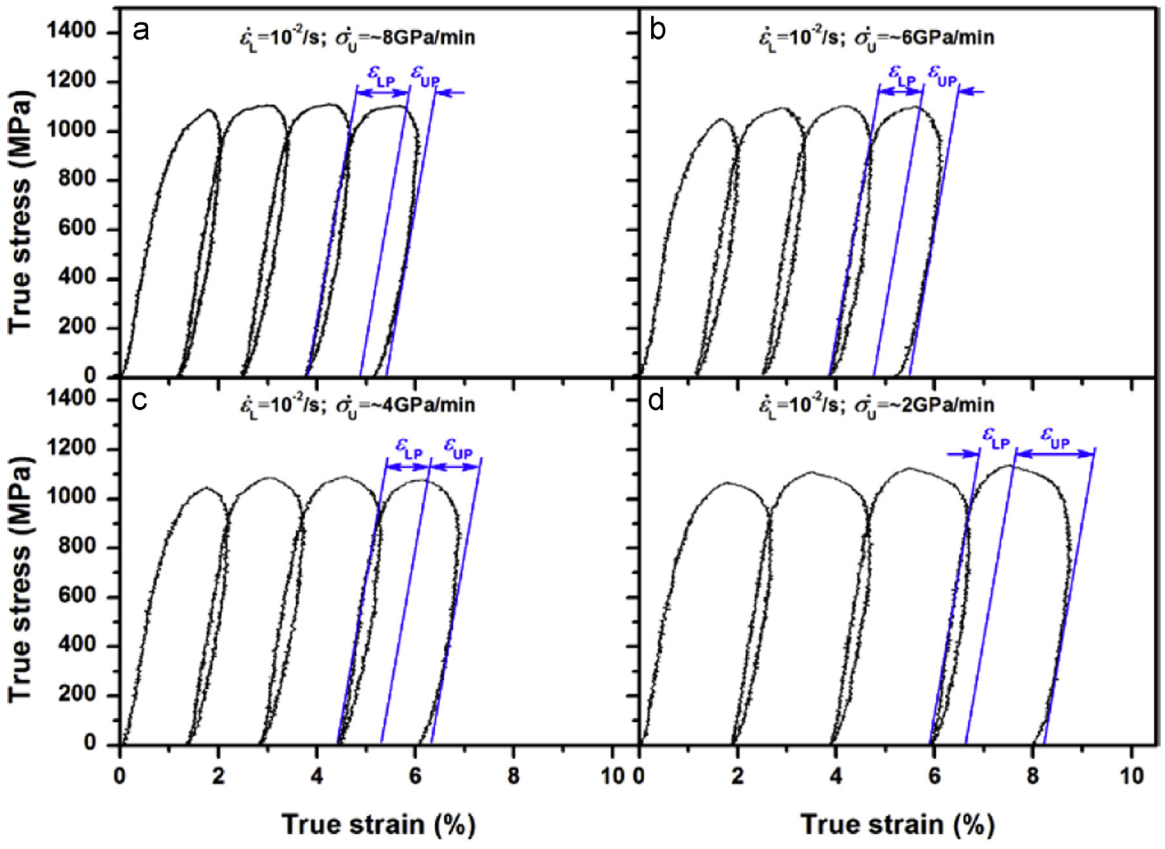

Fig. 2. Compressive cyclic true stress–strain curves of the NC-Cu for the same loading strain rate and four different unloading stress rates.

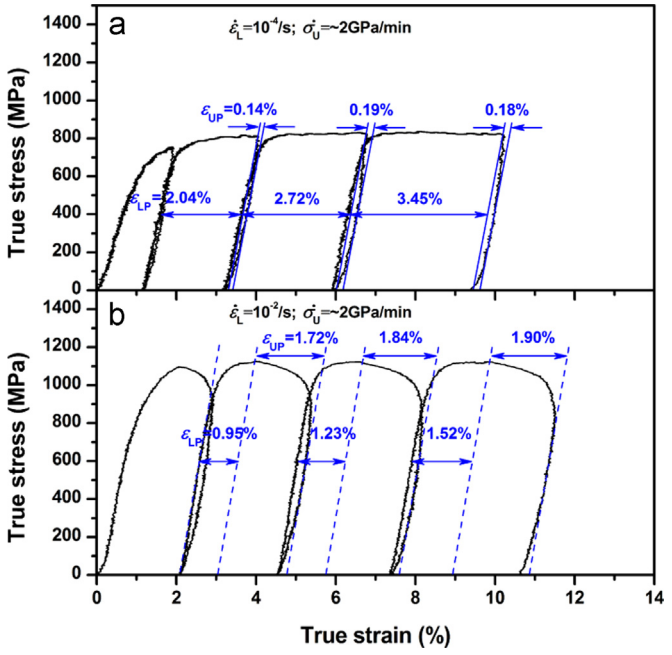

Fig. 3. Compressive cyclic true stress–strain curves of the NC-Cu for different loading strain rates and the same unloading stress rates with increasing loading strain in every cycle step by step.

the same geometric dimensions as the NC-Cu specimens. The typical results in Fig. 5 show that the CG-Cu specimens do not show plastic deformation during unloading, regardless of loading and unloading rates. Their unloading lines are strictly elastic and superposed with the reloading lines. The plastic flow parts of the stress–strain curves in these two cases are not affected by the loading–unloading histories and coincide closely with the monotonous flow curve.

3.2. Dislocation stress field and stress relaxation behavior

Based on the concept of thermally activated plastic flow [21], the applied stress σ for dislocation movement can be described by two components, i.e., athermal long-range internal stress σ_i and thermal short-range effective stress σ^*, in the form of $\sigma = \sigma_i + \sigma^*$. For NC metals, σ_i arises from the inhomogeneous distribution of dislocations inside a grain, σ^* reflects the interactions of gliding dislocations with GBs and is responsible for the dependence of σ on strain rate and temperature [22,23]. To present a quantitative explanation for the unloading plastic deformation behavior observed here, we determined these two components by performing the incremental unloading test [24] on the identical NC-Cu specimens (note that σ^* and σ_i are two necessary magnitudes in the following calculations of dislocation absorption probability and dislocation storage density).

Fig. 6(a) shows the true stress–strain curves for all specimens tested. Fig. 6(b) shows the corresponding true stress–time curves for several typical cases and the three true stress–time curves at higher $\dot{\varepsilon}_L$ are presented in the inset of Fig. 6(b). In the relaxation-incremental loading regime, a pronounced rate-dependent flow stress is observed, which can be evaluated by the strain rate sensitivity ($m = \partial \log \sigma_L / \partial \log \dot{\varepsilon}_L$) and apparent activation volume ($v^* = \sqrt{3}\, kT(\partial \ln \dot{\varepsilon}_L / \partial \sigma_L)$). The results in Fig. 6(c) show that the $\log \sigma_L$ – $\log \dot{\varepsilon}_L$ curves exhibit two distinct linear regimes with their average slopes (i.e., m) for the flow stresses of ε_{LP} = 0.2% and 1.0% at $\dot{\varepsilon}_L \leq 10^{-2}$/s are 0.097 and 0.088, and at $\dot{\varepsilon}_L \geq 10^{-2}$/s are 0.044 and 0.036, respectively. The corresponding v^* are 5.9b^3 and 6.6b^3 at

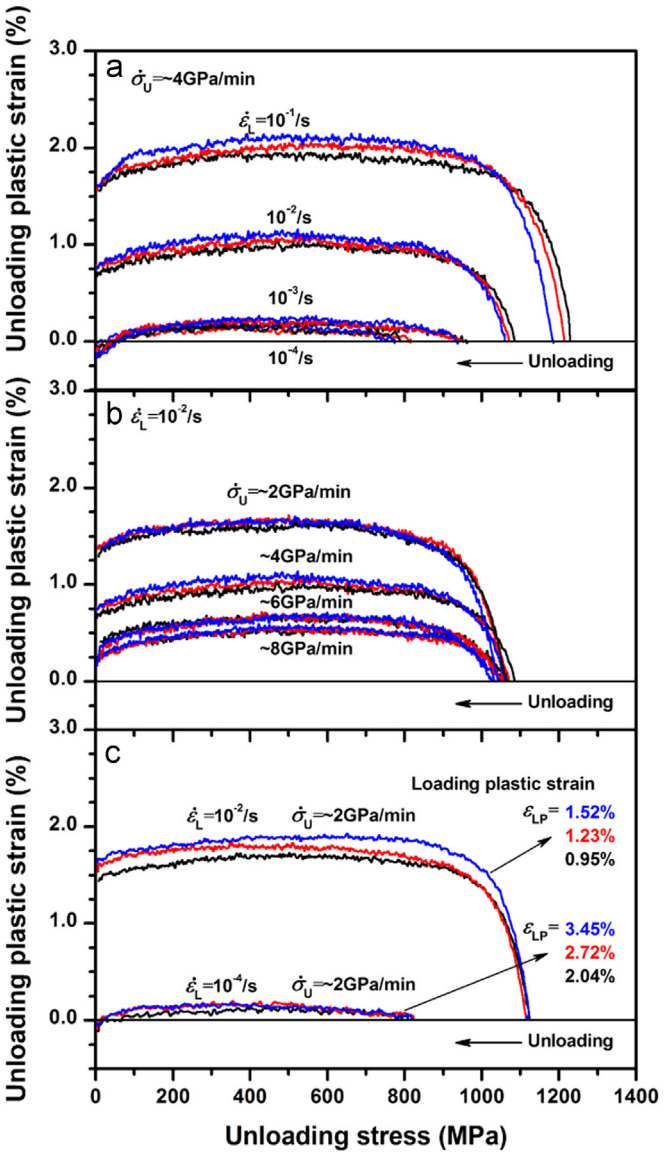

Fig. 4. Variation of the unloading plastic strain with the unloading stress of NC-Cu for different loading strain rates (a), unloading stress rates (b) and loading strains (c) derived from Figs. 1–3.

$\dot{\varepsilon}_L \leq 10^{-2}$/s, and 9.6$b^3$ and 9.2b^3 at $\dot{\varepsilon}_L \geq 10^{-2}$/s, respectively. Such changes in m and v^* agree well with our previous results obtained in the monotonous compressive test on the same NC-Cu [20], implying that a transition of the deformation mechanism occurs across the critical $\dot{\varepsilon}_L = 10^{-2}$/s with increasing strain rate, i.e., from a combination of the thermally activated GB sliding and the dislocation emission–absorption in GBs to one dominated mainly by the dislocation activity.

In the relaxation-incremental unloading regime, the stress relaxes rapidly in the first relaxation interval with a much higher rate at higher $\dot{\varepsilon}_L$ than that at lower $\dot{\varepsilon}_L$, but reaches a similar level for all specimens tested in spite of their considerably different stress values at the initial unloading point. The stress drop at the highest $\dot{\varepsilon}_L$ is $\Delta\sigma_U = \sim 800$ MPa, which is far larger than that at the lowest $\dot{\varepsilon}_L$ ($\Delta\sigma_U = \sim 70$ MPa). In the subsequent relaxation intervals, the stress relaxation rate or average slope of the stress–time curves becomes small and changes from a negative value at a higher stress level to a positive one at a lower stress level. This implies the existence of the internal stress σ_i, namely, the stress corresponding to the zero slope value of the stress–time curves

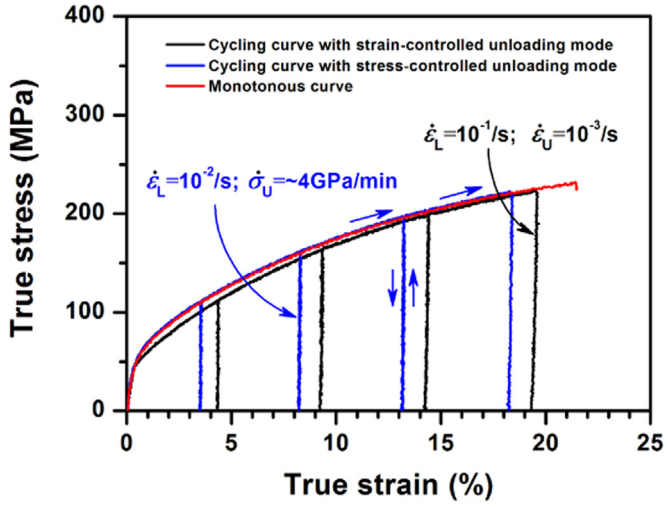

Fig. 5. Compressive cyclic true cyclic stress–strain curves of the CG-Cu for different loading strain rates and unloading stress rates and a monotonous stress–strain curve.

[24,25]. By fitting the stress–time data in every relaxation interval (platform), we obtain the average slope, and then plot it as a function of the corresponding stress level to find σ_i for all specimens tested. The variations of the resulting σ_i and the corresponding effective stress $\sigma^* = \sigma_L - \sigma_i$ with $\dot{\varepsilon}_L$ is shown in Fig. 6(d). One can see that σ_i remains approximately constant and has an average value of ~426 MPa, while σ^* monotonically increases with increasing $\dot{\varepsilon}_L$. In the entire $\dot{\varepsilon}_L$ range tested, the ratio of σ^*/σ_i increases from ~0.5 to ~2.5, which is far larger than the value (σ^*/σ_i=~0.3) obtained from the strain dip test on electrodeposited NC-Ni (d=~30 nm) [16]. The larger values of σ^*/σ_i coincide with the higher m of our NC-Cu. Specifically, the independent strain rate σ_i confirms its athermal nature and the increased σ^* with increasing $\dot{\varepsilon}_L$ can be correlated with the increased density of stored dislocations in the loading regime, as will be discussed below. In addition, our incremental unloading test also indicated that σ_i is less affected by $\dot{\varepsilon}_L$ for the present NC-Cu.

3.3. Microstructure observation after cyclic deformation

Typical TEM images of the as-brush-plated NC-Cu specimen and the NC-Cu specimens after compressive cyclic deformation with the lowest and highest loading strain rates, i.e., $\dot{\varepsilon}_L = 10^{-4}$/s and 10^{-1}/s, and the same unloading stress rate of $\dot{\sigma}_U$ = ~4 GMPa/min are displayed in Fig. 7(a), (b) and (c), respectively. The corresponding statistical results regarding the average grain size are obtained from the TEM images (containing ~500 grains), following the procedure in Refs. [26,27]. It is interesting to find that the average grain size of the NC-Cu specimen deformed at the lowest $\dot{\varepsilon}_L$ increases to ~34 ± 10 nm, while that at the highest $\dot{\varepsilon}_L$ reduces to ~18 ± 5 nm, from ~25 ± 5 nm of the as-brush-plated NC-Cu specimen, as shown in Fig. 7(d), (e) and (f), respectively. These results indicate that slower loading deformation makes the grains slightly coarsen, while faster loading deformation refines slightly the grains.

4. Discussions

4.1. Size- and rate-dependent dislocation storage

For the present NC-Cu, the dislocation emission–absorption process and GB-mediated mechanisms such as thermally activated GB sliding are likely to switch on in the loading regime

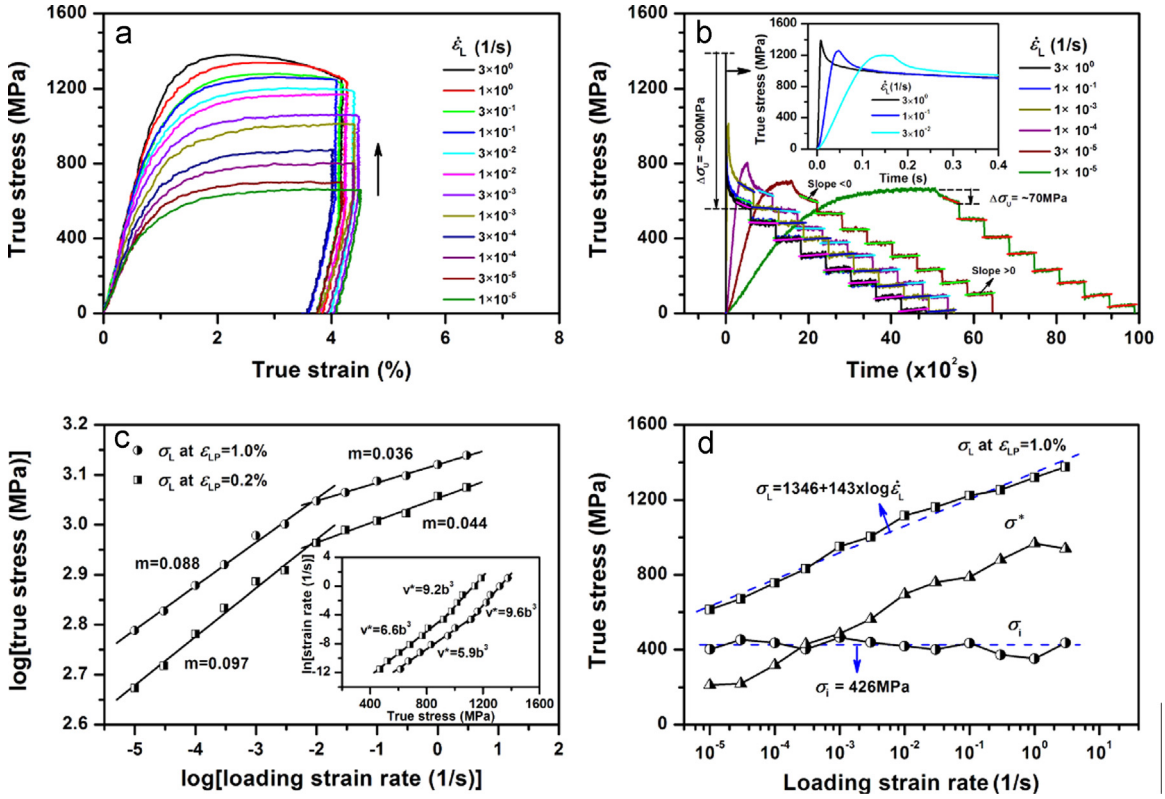

Fig. 6. True stress–strain curves (a), typical true stress–time curves (b), logarithm true stress–loading strain rate curves for measuring the strain rate sensitivity and activation volume (c), and the variation of the flow stress, effective stress and internal stress with loading strain rate (d) of the NC-Cu obtained from the incremental unloading tests.

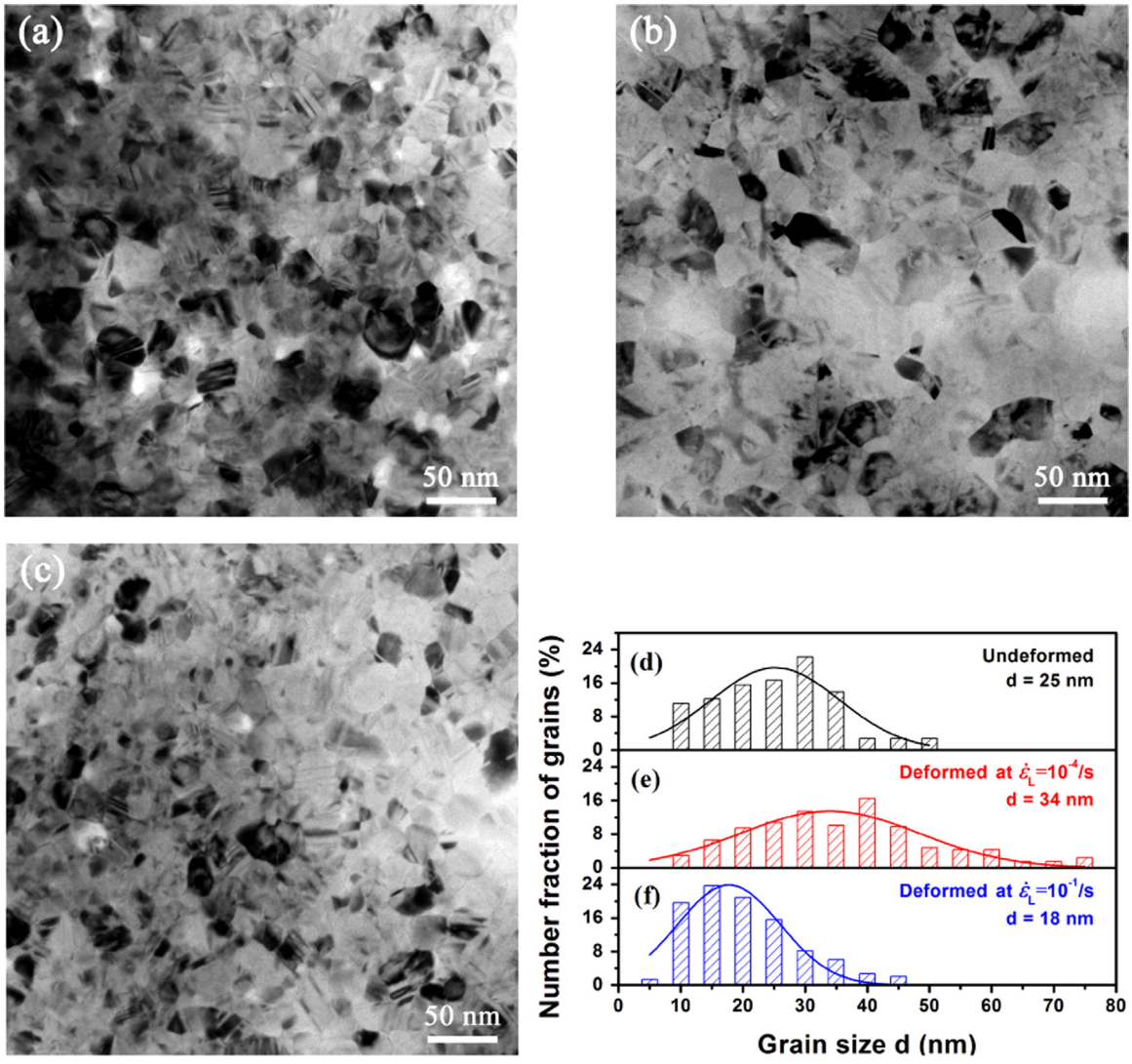

Fig. 7. Typical TEM images taken from the NC-Cu specimens before (a) and after the compressive cyclic deformation at loading strain rates of 10^{-4}/s (b) and 10^{-1}/s (c) and unloading stress rate of ~4 GPa/min, and (d–f) is the corresponding statistical results of grain size distribution.

considering its grain size and the range of $\dot{\varepsilon}_L$ used in this test [1,2,8,20,28,29]. At lower $\dot{\varepsilon}_L$, the GB sliding tends to preferentially operate due to its low threshold stress and sufficient time during loading and even becomes dominant mechanism accommodating applied plastic strain. However, as $\dot{\varepsilon}_L$ increases, this GB sliding process is suppressed due to the increased difficulty or insufficient time for atomic diffusion. A much higher stress level is thus needed for the GB sliding process to proceed until a critical stress level at which the dislocation emission–absorption process is activated effectively. Once dislocations are emitted from the GB sources, e.g., GB ledges, they propagate across the grain and are finally absorbed in the opposite GBs. This rate-dependent dislocation absorption process involves the rearrangement of dislocation structures at/near GBs with the assistance of atomic diffusion [22,30,31]. If the dislocation emission rate overwhelms the absorption rate, a rate-dependent storage or accumulation of dislocations will occur inside the grains [10,18,32]. Upon unloading, these stored dislocations would continue to propagate forward and result in a continuous increase of plastic strain when they are absorbed in the opposite GBs. Considering that an absorbed dislocation with length L (scaling with d) is controlled by atomic jump or migration from the dislocation core to the GB, Carlton and Ferreira [18] constructed a model of d- and $\dot{\varepsilon}_L$-dependent statistical absorption of dislocations by GBs (termed as SAD model hereafter). By carefully constructing the required variables, such as the σ^* and $\dot{\varepsilon}_L$, and combining the Bernoulli distribution function, a theoretical expression for the probability of dislocations being absorbed by GBs was derived. This expression was successfully used to quantitatively interpret the inverse Hall–Petch effect of strength and the dependence of this effect on $\dot{\varepsilon}_L$ and temperature.

Next, we will correlate $\dot{\varepsilon}_L$ with the density of stored dislocations during loading based on the SAD model [18] and the GB-ledge model proposed by Li [19]. From the GB-ledge model, a parameter ω can be used to characterize the ability of GBs to emit dislocations in a polycrystalline metal with a grain size d. Physically, ω corresponds to the total number of emitted dislocations from the unit length of GB or the total length of emitted dislocations from the unit area of GB. The density of emitted dislocations ρ from GBs can be connected with ω by [19]

$$\rho = 3\omega/d \tag{1}$$

Additionally, ρ can be correlated with the loading plastic strain ε_{LP} via $\rho = \varepsilon_{LP}/(bl)$, where b is the magnitude of Burgers vectors and l is the dislocation mean free path scaling with d. According to the dislocation strain hardening model [19,33] the Hall–Petch relation for the flow stress at given ε_{LP} can be given by

$$\sigma_L = \sigma_0 + M\alpha Gb\rho^{1/2} = \sigma_0 + M\alpha Gb\sqrt{3\omega}\, d^{-1/2} = \sigma_0 + Kd^{-1/2} \tag{2}$$

where σ_0 and $K = M\alpha Gb\sqrt{3\omega}$ are the Hall–Petch intercept (friction stress) and slope, respectively, M is Taylor factor, α is a dimensionless material constant (~0.2–0.5) [19,33], G is the shear modulus. The Hall–Petch relation has been experimentally established in NC-Cu until a grain size down to about 10 nm [34]. From Eq. (2), ρ can be expressed

$$\rho = (\frac{\sigma_L - \sigma_0}{M\alpha Gb})^2 = (\frac{K}{M\alpha Gb})^2 \frac{1}{d} \quad (3)$$

Comparing Eq. (2) with the relation of $\sigma_L = 1346 + 143 \log \dot{\varepsilon}_L$ obtained by fitting the experimental flow stress data at $\varepsilon_{LP} = 1.0\%$ in Fig. 6(d), an empirical relation of $K = 6080 + 715 \log \dot{\varepsilon}_L$ for the present NC-Cu can be obtained using $d = 25$ nm and $\sigma_0 =$ ~130 MPa derived from the nanoidentation test on the brash-plated NC-Cu [35]. This $K - \log \dot{\varepsilon}_L$ relation is found to be similar to that obtained in the nanoidentation test on the same NC-Cu ($K = 4641 + 756 \log \dot{\varepsilon}_L$ [35]). ρ as a function of $\dot{\varepsilon}_L$ can thus be determined from Eq. (3).

Considering that the dislocation absorption is controlled by an atomic jump or migration from the dislocation core to a GB, a theoretical model for the probability of dislocation absorption by GBs P_L was developed by Carlton and Ferreira (the SAD model) [18]. The SAD model can be written as

$$P_L = [1 - (1 - p)^I]^J = \{1 - [1 - \exp(X)]^I\}^J \quad (4)$$

where $X = -(\Delta G + \tau^* b^3)/(kT)$, $p = \exp(X)$ is the probability value of a dislocation being successfully absorbed by GB, $I = bv/(M\dot{\varepsilon}_L d)$ is the number of a dislocation attempting to jump GB and being absorbed during a success absorption, $J = \omega d$ is the total number of atoms in a dislocation participating in the absorption process or the total number of dislocations emitted from a GB, ΔG is the activation energy for atomic migration from a dislocation core to a GB, k is the Boltzmann constant, T is temperature, $\tau^* = \sigma^*/M$ is the effective shear stress, v is Debye frequency. In Eq. (4), the term $(1 - p)^I$ denotes the probability of a dislocation failing to be absorbed after I number of attempts, and the term $[1 - (1 - p)^I]^J$ is thus the probability of all J dislocations being absorbed by the GB; both terms are assumed to follow the Bernoulli distribution. If $P_L = 0$, emitted dislocations are completely stored inside the grain (GBs are opaque). In contrast, if $P_L = 1$, emitted dislocations are completely absorbed by GBs (GBs are transparent). Considering the contribution of P_L in Eqs. (1) and (2), the density of stored dislocations and the corresponding flow stress in the loading regime can be respectively written as

$$\rho_L = \rho(1 - P_L) = 3\omega\{1 - \{1 - [1 - \exp(X)]^I\}^J\} d^{-1} \quad (5)$$

$$\sigma_L = \sigma_0 + M\alpha Gb\rho_L^{1/2} = \sigma_0 + M\alpha Gb\sqrt{3\omega\{1 - \{1 - [1 - \exp(X)]^I\}^J\}}\, d^{-1/2} \quad (6)$$

Inserting the material parameters and experimental data listed in Table 1 into Eqs. (5) and (6), P_L and ρ_L for different d and ΔG values were calculated and are plotted in Fig. 8 as a function of $\dot{\varepsilon}_L$. It can be seen that the P_L versus $\dot{\varepsilon}_L$ plot can be divided into three distinct regions (regions I, II and III, Fig. 8(a) and (b)). In region I, the emitted dislocations are completely absorbed by GBs ($\rho_L = 0$ due to $P_L = 1$); in region II, the emitted dislocations are partly absorbed by GBs ($\rho_L > 0$ due to $0 < P_L < 1$); in region III, the emitted dislocations are completely stored inside the grains ($\rho_L > 0$ due to $P_L = 0$). Furthermore, as d and ΔG decreasing, region II shifts toward to a higher $\dot{\varepsilon}_L$ (Fig. 8(a) and (b)), indicating that much higher $\dot{\varepsilon}_L$ is needed to ensure the effective dislocation storage. In region III, ρ_L increases as d decreases (Fig. 8(c)), but is not affected by ΔG (Fig. 8(d)), implying that ρ_L is controlled only by dislocation emission because dislocation absorption does not occur in this region ($P_L = 0$).

Table 1
Material parameters and experimental data.

Parameter	Value
Taylor factor	$M = 3.06$
Shear modulus	$G = 48.3$ GPa
Burgers vector	$b = 0.1476$ nm
Temperature	$T = 298$ K
Boltzmann constant	$k = 1.38 \times 10^{-23}$ J/K
Debye frequency	$v = 7.2 \times 10^{12}$/s [30]
Friction stress	$\sigma_0 = 130$ MPa
Internal stress	$\sigma_i = 426$ MPa
Material constant	$\alpha = 0.3$ [19,31]

4.2. Deformation mechanism transition

The significant strain rate dependence of ρ_L shown in Fig. 8 (c) and (d) indicates again a gradual transition in the plastic deformation mechanism [20]. At low $\dot{\varepsilon}_L$ (regions I and II), although the dislocation emission–absorption process contributes to plastic flow, the GB sliding is the main mechanism dominating plastic flow. In contrast, at high $\dot{\varepsilon}_L$ (region III), plastic deformation is mainly controlled by dislocation activities. Such a transition in the plastic deformation mechanism predicted by the variation in ρ_L has been supported by the significant changes in the m and v^* values shown in Fig. 6(c). The approximately doubled m at $\dot{\varepsilon}_L \le 10^{-2}$/s as compared with the value at $\dot{\varepsilon}_L \ge 10^{-2}$/s stems from the contribution of GB sliding with m of ~0.5 [36] because dislocation activities usually lead to a relatively smaller m [20].

According to $\dot{\varepsilon}_L$ at the transition point of m ($\dot{\varepsilon}_L =$ ~10^{-2}/s), ΔG for the present NC-Cu can be approximately determined by a trial calculation, which yields a value of $\Delta G =$ ~0.7 eV. This ΔG value falls in the range of ~0.6–0.95 eV reported for polycrystalline Cu [32]. Taking ΔG=0.7 eV, σ_L as a function of $\dot{\varepsilon}_L$ for our NC-Cu was calculated by using Eq. (6) and is compared with the experimental data, as shown in Fig. 9. As expected, the calculated σ_L agrees well with the experimental value at $\dot{\varepsilon}_L \ge 10^{-2}$/s, but is lower than the experimental value at $\dot{\varepsilon}_L \le 10^{-2}$/s. This discrepancy between the calculation and experiment is caused by the fact that the contribution of GBs sliding to σ_L is not considered in Eq. (6). For the plastic flow mediated by GB or dislocation activities or both, the flow stress scales also with $\dot{\varepsilon}_L$ and can be given by [25,37–39]

$$\sigma_L = A + B(kT/v^*)\log \dot{\varepsilon}_L \quad (7)$$

where v^* reflects the contributions of GB or dislocation activities or both, A and B are constants. A and B depend on loading strain and can be determined by comparing with the experimental σ_L data in Fig. 6(d) ($\sigma_L = 1346 + 143 \log \dot{\varepsilon}_L$). σ_L at $\dot{\varepsilon}_L \le 10^{-2}$/s was obtained by using Eq. (7) and is also presented Fig. 9. The results in Fig. 9 suggest that σ_L at $\dot{\varepsilon}_L \ge 10^{-2}$/s is mainly governed by the dislocation activities (Eq. (6)), while σ_L at $\dot{\varepsilon}_L \le 10^{-2}$/s is mainly controlled by the GB-mediated process (Eq. (7)). The above arguments are well supported by the change in v^* with $\dot{\varepsilon}_L$ (Fig. 6(c)).

4.3. Dislocation structure relaxation and unloading plastic deformation

In the loading regime, the stored dislocations at higher loading strain rate or higher applied stress tend to relax upon unloading via their absorption/annihilation in GBs. This process occurs because a higher stress level is still maintained in the initial unloading stage, as is confirmed by the incremental unloading test (Fig. 6(b)). Such a rapid stress drop in the first relaxation interval for the specimens deformed at higher $\dot{\varepsilon}_L$ cannot be connected by

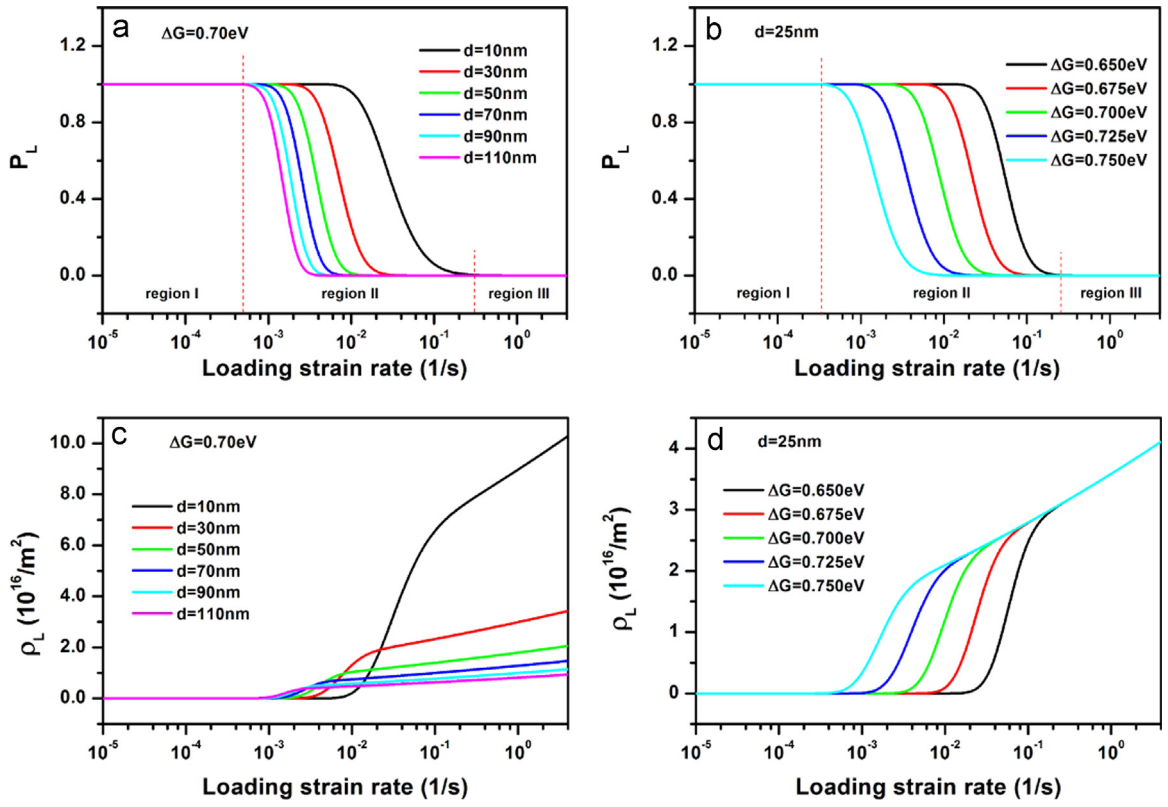

Fig. 8. Variations of the probability (a,b) and density (c,d) of stored dislocations of the NC-Cu with loading strain rate for different grain sizes.

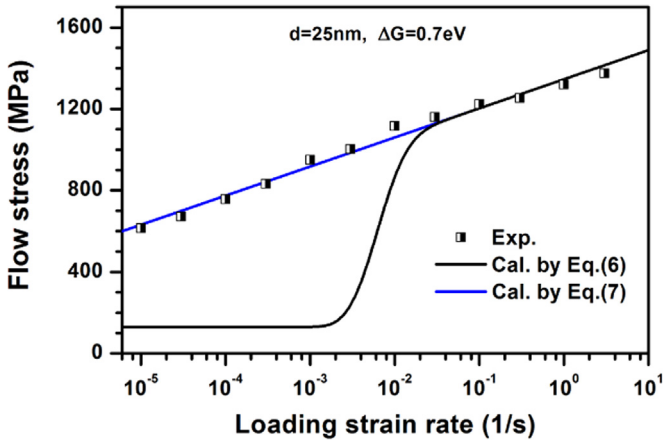

Fig. 9. Variations of the flow stress at 1 % plastic strain with loading strain rate of the NC-Cu obtained from the incremental unloading test and from the calculations by using Eqs. (6) and (7).

the GB-mediated process. Instead, the GB-mediated process is likely to occur and is responsible for slow stress relaxation at lower $\dot{\varepsilon}_L$, for which fewer dislocations are stored in the loading regime, as shown in Fig. 8(c).

The significant unloading plasticity observed in the compressive cyclic test is a result of the relaxation of dislocation structures generated in the loading regime. Similar to that in the loading regime, the dislocation activities in the unloading regime are also controlled by the effective stress σ^*. When the unloading stress σ_U is reduced to a level above σ_i, $\sigma^* \geq 0$ (where σ_i remains unchanged as indicated by our incremental unloading test (σ^* relaxes prior to σ_i)). As the driving force, this positive σ^* would push the stored dislocations to move forward and make them be absorbed by opposite GBs, producing a forward plastic strain, i.e., the unloading plastic strain ε_{UP}. In the initial unloading stage, larger σ^* (or larger σ_U) would result in a higher increasing rate of ε_{UP} with decreasing σ_U (Fig. 4). When σ_U is reduced to a level equating to σ_i, $\sigma^* = 0$. In this case, the dislocation absorption process ceases, ε_{UP} no longer increases and reaches its maximum value. When σ_U is further reduced to a level below σ_i, a negative stress difference $\Delta\sigma = \sigma_U - \sigma_i < 0$ is generated. This stress difference would cause the recovery of plastic strain ε_{RP} by promoting the reverse local GB sliding and diffusion and/or the reverse dislocation absorption in the original GBs [10,11,16,17,40] until the complete relaxation of σ_i. This plastic recovery process has been reported in cyclic testing on some nanostructured metals [10,11,17]. Due to larger internal stress caused by the inhomogeneous grain size distribution and relatively longer unloading time, the recovery of plastic strain is considerably significant in these materials [10,11,17]. For our NC-Cu, however, the recovery of plastic strain is small (ε_{RP} < ~0.5 %) due to the relatively rapid unloading.

4.4. Unloading plastic strain and dislocation structure stability

The plastic strain produced in the unloading regime depends on the density of dislocations that are absorbed by GBs in the unloading regime ρ_U. Apparently, ρ_U is related to ρ_L and, like ρ_L, is also controlled by the probability of dislocation absorption by GBs in the unloading regime P_U. Based on similar consideration to that in the loading regime, ρ_U can be given by

$$\rho_U = \rho_L P_U = \rho(1 - P_L)P_U \tag{8}$$

where P_U has the same form as P_L (Eq.(5)) and ρ_U depends on unloading strain rate $\dot{\varepsilon}_U$ as indicated by Eq. (4). Using the material parameters and experimental data in Table 1, ρ_U as a function of $\dot{\varepsilon}_L$ for different $\dot{\varepsilon}_U$ is calculated by Eq. (8) and typical results for the NC-Cu and CG-Cu specimens are shown in Fig. 10(a) and (b). It is found that for the NC-Cu specimens, ρ_U varies with $\dot{\varepsilon}_L$ in a similar way to ρ_L and increases as $\dot{\varepsilon}_U$ decreases from $\rho_U \approx 0$ at $\dot{\varepsilon}_U \geq 10^{-1}$/s to $\rho_U = \rho_L$ at $\dot{\varepsilon}_U \leq 10^{-3}$/s. The variation of ρ_U with $\dot{\varepsilon}_U$ for a given $\dot{\varepsilon}_L$ of

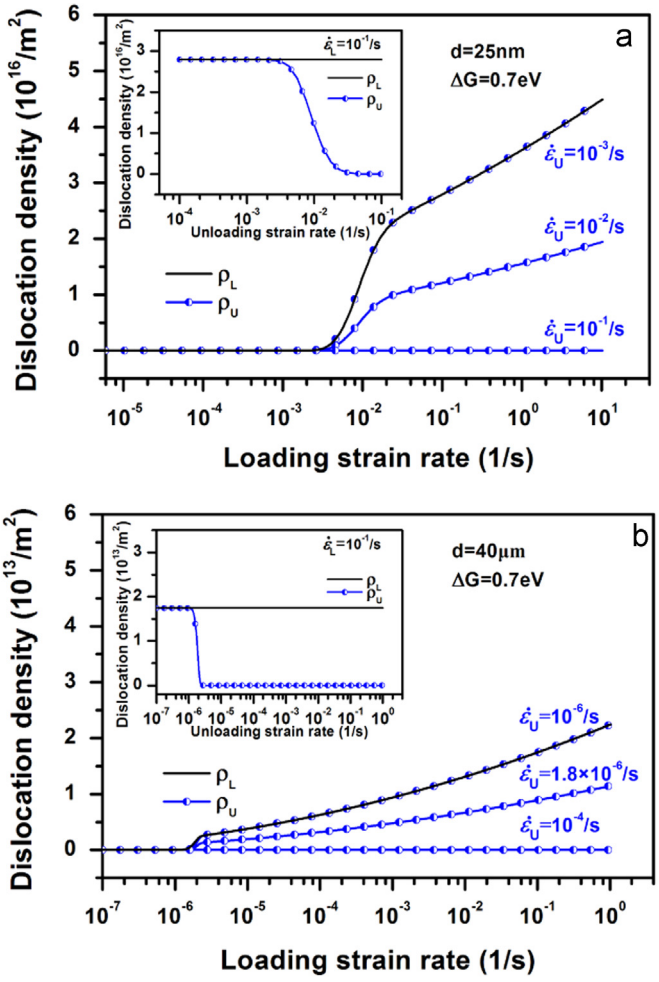

Fig. 10. Variation of the density of stored dislocations of the NC-Cu (a) and CG-Cu (b) in the loading regime with loading strain rate and variations of the density of dislocations absorbed in the unloading regime with unloading strain rate. The insets in (a) and (b) are variations of the density of stored dislocations of the NC-Cu and CG-Cu in the loading regime with loading strain rate of 10^{-1}/s and variations of the density of dislocations absorbed in the unloading regime with unloading strain rates after loading strain rate of 10^{-1}/s.

10^{-1}/s in the inset in Fig. 10(a) reveals further that the stored dislocations during loading are completely absorbed at $\dot{\varepsilon}_U \le 10^{-3}$/s ($\rho_U = \rho_L$) and are completely reserved at $\dot{\varepsilon}_U \ge 10^{-1}$/s ($\rho_U = 0$).

The absorption of the stored dislocations during unloading produces ε_{UP} via shearing the grain or changing the grain shape. ε_{UP} produced by this dislocation absorption process can be estimated by the relation [41]

$$\varepsilon_{UP} = \frac{N}{2\sqrt{3}}\frac{b}{d} = \frac{\rho_U bd}{2\sqrt{3}} \tag{9}$$

where $N_U = \rho_U d^2$ is the total dislocation number that are absorbed by GBs during unloading. The calculations by using Eq. (9) indicate that ε_{UP} for the NC-Cu specimens is very large due to their larger value of ρ_U at lower $\dot{\varepsilon}_U$, while ε_{UP} for the CG-Cu specimens is zero due to $\rho_U = 0$ or $P_U = 0$ at the tested $\dot{\varepsilon}_U$ in spite of the fact that $\rho_L > 0$ as indicated by the calculated results in Fig. 10(b). This means that although a high density of dislocations can be stored in the CG-Cu specimens during loading, the GB absorption process does not occur during unloading. It can explain why the CG-Cu specimens do not exhibit the detected unloading plasticity (Fig. 5).

Because the resultant unloading strain would be constrained by the strain-controlled unloading mode as stated above, the calculated ε_{UP} by Eq. (9) cannot be compared directly with the present experimental data obtained in the stress-controlled unloading mode. However, it is noted that the variations of ε_{UP} with $\dot{\varepsilon}_L$ and $\dot{\varepsilon}_U$ predicted by Eq. (9) are well consistent with the experimental results in the magnitude and tendency. For example, the largest ε_{UP} calculated at the loading strain rates of $\dot{\varepsilon}_L = 10^{-2}$/s and $\dot{\varepsilon}_L = 10^{-1}$/s and the lowest unloading strain rate of $\dot{\varepsilon}_U < 10^{-3}$/s is $\varepsilon_{UP} = 1.85\%$ and $\varepsilon_{UP} = 2.97\%$, which are slightly larger than the experimental values of $\varepsilon_{UP} = 1.61\%$ and $\varepsilon_{UP} = 2.01\%$ obtained at the same $\dot{\varepsilon}_L$ and the lowest unloading stress rate of $\dot{\sigma}_U$=2 GPa/min and $\dot{\sigma}_U$=4 GPa/min, respectively.

Apart from the loading and unloading rates, the above ε_{UP} would also affected by other possible factors. Firstly, the creep behavior mediated by the GB sliding and/or GB diffusion occurred in the unloading regime would lead to an increase in ε_{UP}, especially at a lower unloading rate. Secondly, higher stress level holds in the initial unloading stage might emit new dislocations from GBs, which are contribute to ε_{UP} after absorption by the opposite GBs. Thirdly, some dislocations nearby GB sources would glide back and be absorbed by the GBs where they originated, which reduces ε_{UP} by producing negative value of ε_{UP}. Finally, twin structures existed in the present NC-Cu specimen including those formed during the brush-plated deposition and generated during the cyclic deformation can impede the absorption processes of stored dislocations, which would lead to a decrease in ε_{UP}. Obviously, the last two factor might have more contribution to the ε_{UP} in the experimental process, resulting in its slightly low value as compared that of the calculation. Such the role of interaction between the dislocations and nano-scaled twins in controlling plastic deformation and stabilizing deformation structure should be reasonably considered.

4.5. *Deformation structure evolution during cyclic deformation*

Our high resolution TEM observations results indicate that TBs-mediated processes are closely correlated with the evolution of deformation structures, i.e., the grain growth at lower $\dot{\varepsilon}_L$ and the grain refinement at higher $\dot{\varepsilon}_L$, which is described as following.

One possible mechanism for grain refinement at higher $\dot{\varepsilon}_L$ is the intersection of twins, i.e., “secondary” twins traverse “primary” twins [42,43], which divide the grain into several parts, as shown in Fig. 11(a). More details about the underlying mechanism for twin intersections can be found in Refs. [42,43]. Indeed, as observed from Fig. 11(a) and (b), the intersection of twins that can transform the coherent twinning boundaries (CTBs) into incoherent twinning boundaries (ITBs), even into GBs, and this process has been determined in the previous experiments on Cu–Zn alloy [43]. Specifically, more dislocation emission at higher $\dot{\varepsilon}_L$ accompanied with more severe dislocation accumulation is more preferred to trigger the activation of secondary twins by partial dislocation emissions from the other side of the TB [44]. Furthermore, at higher $\dot{\varepsilon}_L$, the random activated partials process would more effectively relieve high local stress concentration [27,45], which in turn leads to more significant intersection of twins as well as dislocation–TB interactions. Notably, the TBs/GBs intersection is a critical development for the occurrence of the grain subdivision, in which further deformation transforms the TBs into GBs via dislocation–TBs interactions [43,46].

On the other hand, lower $\dot{\varepsilon}_L$ leads to a smaller probability of dislocation emission from GBs and weaker the dislocation accumulation. Unlike the case at higher $\dot{\varepsilon}_L$, the applied plastic strain is more favored to be accommodated by random dislocation emission in lieu of partial accumulation [27,45,47]. The detwinning process accomplished via the collective glide of multiple twinning dislocations is likely the dominant mechanism that allows grain growth at a low stress level because the diffusion-based mobility is inactive at room temperature [46,48–50]. Brons and coworkers

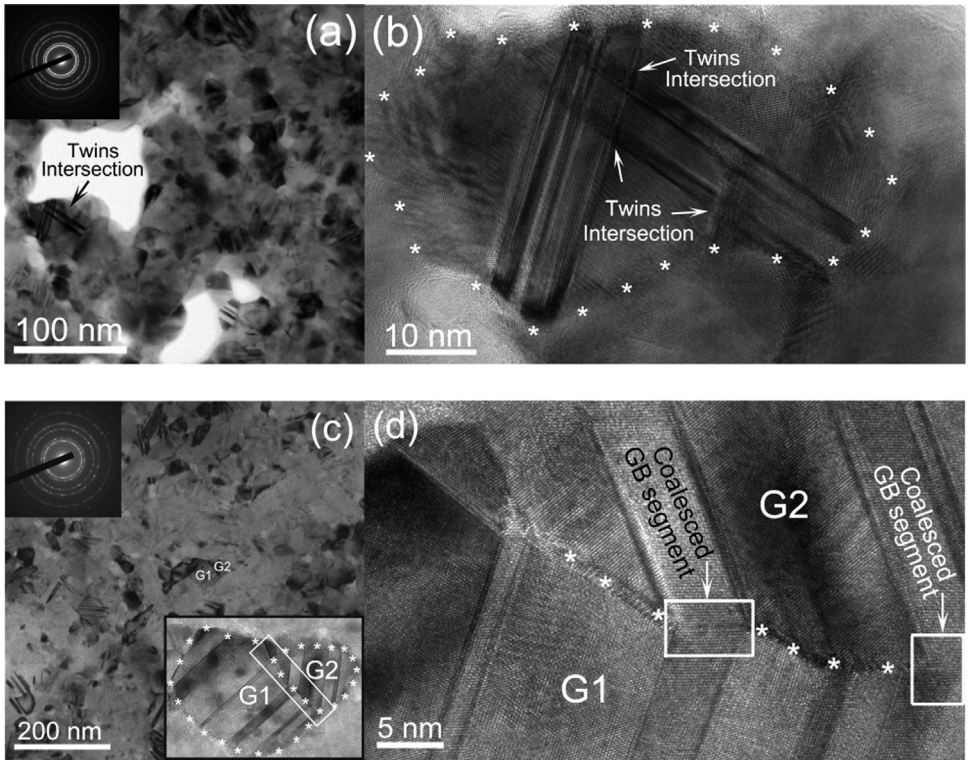

Fig. 11. Typical TEM images of the NC-Cu deformed (a,b) at high loading strain rate of 10^{-1}/s showing intersection of twins and (c,d) at low loading strain rate of 10^{-4}/s showing two small-sized grains (G1, G2) coalescence via the twinning/detwinning process. Upper insets in (a,c) are the corresponding selected area diffraction patterns, lower inset in (c) is a high magnification view of grains G1 and G2. (b) is the highly magnified view of the twinned grain indicated by arrow in (a) and (d) is the high magnified view of the boxed region of the lower inset in (c), showing coalesced GBs segments as marked by boxes. GBs are marked by white stars.

[48] observed significant grain coarsening, prevalent Σ7 subgrain formation and a decrease in TBs in the deformed NC-Cu thin films with as-deposited Σ3 TBs, which indicates that detwinning triggers grain growth. To some extent, the detwinning process can be treated as the reversible process of twinning. Thus, twinning likely causes the grain growth. Indeed, we observed two smaller grains coalesce together to form a larger grain through twinning/detwinning via ITBs motion that produces zero strain, as shown in Fig. 11(c). It appears that localized GBs between these two small grains disappear or coalesce, as marked by white boxes in Fig. 11 (d).

5. Conclusions

In this work, we report the experimental finding of significant plastic deformation that emerges in the unloading regime and its strong dependence on loading and unloading rates in NC-Cu under loading–unloading compressive cyclic test at room temperature. This plastic deformation behavior during unloading, together with the TB-mediated evolution of deformation structures, not only benefits our understanding of unique behavior of highly mobile dislocations in NC metals, but also sheds light on the controllability of plastic deformation and the stability of deformation structure. The main conclusions are summarized as follows:

(1) The significant plastic deformation behavior during unloading and its strong dependence on loading and unloading rates arises from the rapid absorption of dislocations accumulated during loading, which is quantitatively interpreted by performing the incremental unloading test and developing a relationship between the dislocation density and the loading and unloading rates based on the models of the statistical absorption of dislocations by GBs and the dislocation emission from GB ledges.
(2) There is a critical loading strain rate for the deformation mechanism transition: below this loading strain rate, the GB-mediated processes switch on, while above this loading strain rate, the dislocation activity dominates the plastic deformation behavior.
(3) The dislocations-stimulated detwinning process facilitates the grain growth at lower loading strain rates, while the dislocations-triggered TB-to-GB transition process, i.e., twins intersection, leads to the grain refinement at higher loading strain rates.

Acknowledgments

This work was supported by the National Natural Science Foundation of China (Grant nos. 51371089, 50871046, 51321003, 51201123 and 51271152) and the Foundation of National Key Basic Research and Development Program of China (Grant nos. 2010CB631001 and 2010CB631003). JYZ thanks the China Postdoctoral Science Foundation (2012M521765) and Shaanxi Province Postdoctoral Scientific Research Projects for their contributions towards financial support. This was also supported by the State Key Laboratory for Mechanical Behavior of Materials (Grant no. 20121205). JYZ thanks the support of The Project Supported by Natural Science Basic Research Plan in Shaanxi Province of China (Program no. 2015JM5158).

References

[1] H. Van Swygenhoven, Science 296 (2002) 66–67.
[2] J. Schiøtz, K.W. Jacobsen, Science 301 (2003) 1357–1359.

[3] V. Yamakov, D. Wolf, S.R. Phillpot, A.K. Mukherjee, H. Gleiter, Nat. Mater. 3 (2004) 43–47.
[4] D. Wolf, V. Yamakov, S.R. Phillpot, A. Mukherjee, H. Gleiter, Acta Mater. 53 (2005) 1–40.
[5] H. Van Swygenhoven, P.M. Derlet, A.G. Froseth, Acta Mater. 54 (2006) 1975–1983.
[6] R.J. Asaro, S. Suresh, Acta Mater. 53 (2005) 3369–3382.
[7] P. Gu, M. Dao, R.J. Asaro, S. Suresh, Acta Mater. 59 (2011) 6861–6868.
[8] Z.W. Shan, E.A. Stach, J.M. Wiezorek, J.A. Knapp, D.M. Follstaedt, S.X. Mao, Science 305 (2004) 654–657.
[9] K.M. Youssef, R.O. Scattergood, K.L. Murty, J.A. Horton, C.C. Koch, Appl. Phys. Lett. 87 (2005) 091904.
[10] F. Mompiou, D. Caillard, M. Legros, H. Mughrabi, Acta Mater. 60 (2012) 3402–3414.
[11] J. Rajagopalan, C. Rentenberger, H.P. Karnthaler, G. Dehm, M.T.A. Saif, Acta Mater. 58 (2010) 4772–4782.
[12] M.S. Colla, B. Amin-Ahmadi, H. Idrissi, L. Malet, S. Godet, J.P. Raskin, D. Schryvers, T. Pardoen, Nat. Commun. 6 (2015) 5922.
[13] Z. Budrovic, H. Van Swygenhoven, P.M. Derlet, S. Van Petegem, B. Schmitt, Science 304 (2004) 273–276.
[14] Z. Sun, S. Van Petegem, A. Cervellino, K. Durst, W. Blum, H. Van Swygenhoven, Acta Mater. 91 (2015) 91–100.
[15] V. Yamakov, D. Wolf, M. Salazar, S.R. Phillpot, H. Gleiter, Acta Mater. 49 (2001) 2713–2722.
[16] S. Van Petegem, S. Brandstetter, H. Van Swygenhoven, J.L. Martin, Appl. Phys. Lett. 89 (2006) 073102.
[17] J. Rajagopalan, J.H. Han, M.T.A. Saif, Science 315 (2007) 1831–1834.
[18] C.E. Carlton, P.J. Ferreira, Acta Mater. 55 (2007) 3749–3756.
[19] J.C.M. Li, Y.T. Chou, Metall. Mater. Trans. B 1 (1970) 1145–1159.
[20] Z.H. Jiang, H.Z. Zhang, C.D. Gu, Q. Jiang, J.S. Lian, J. Appl. Phys. 104 (2008) 053505.
[21] M. Zaiser, A. Seeger, Dislocations in Solids, vol. 56, Amsterdam, Elsevier (2002), p. 1–100.
[22] Y.M. Wang, A.V. Hamza, E. Ma, Acta Mater. 54 (2006) 2715–2726.
[23] T. Zhu, J. Li, A. Samanta, A. Leach, K. Gall, Phys. Rev. Lett. 100 (2008) 25502.
[24] H. Conrad, Mater. Sci. Eng. A 6 (1970) 265–273.
[25] H. Conrad, Mater. Sci. Eng. A 341 (2003) 216–228.
[26] J.Y. Zhang, G. Liu, R.H. Wang, J. Li, J. Sun, E. Ma, Phys. Rev. B 81 (2010) 172104.
[27] J.Y. Zhang, P. Zhang, R.H. Wang, G. Liu, G.J. Zhang, J. Sun, Phys. Rev. B 86 (2012) 064110.
[28] J.J. Hu, S. Han, G.X. Sun, S.C. Sun, Z.H. Jiang, G.Y. Wang, J.S. Lian, Mater. Sci. Eng. A 618 (2014) 621–628.
[29] Z.H. Jiang, X.L. Liu, G.Y. Li, Q. Jiang, J.S. Lian, Appl. Phys. Lett. 88 (2006) 143115.
[30] N.N. Guo, J.Y. Zhang, P.M. Cheng, G. Liu, J. Sun, Scr. Mater. 68 (2013) 849–852.
[31] F. Mompiou, D. Caillard, M. Legros, Acta Mater. 57 (2009) 2198–2209.
[32] J.Y. Zhang, G. Liu, J. Sun, Int. J. Plast. 50 (2013) 1–17.
[33] U.F. Kocks, H. Mecking, Prog. Mater. Sci. 48 (2003) 171–273.
[34] J. Chen, L. Lu., K. Lu., Scr. Mater. 54 (2006) 1913–1918.
[35] J.W. Mu, S.C. Sun, Z.H. Jiang, J.S. Lian, Q. Jiang, Chin. Phys. B 22 (2013) 037303.
[36] M.A. Meyers, A. Mishra, D.J. Benson, Prog. Mater. Sci. 51 (2006) 427–556.
[37] A.H. Chokshi, Scr. Mater. 61 (2009) 96–99.
[38] H. Hirakata, N. Fukuhara, S. Ajioka, A. Yonezu, M. Sakihara, K. Minoshima, Acta Mater. 60 (2012) 4438–4447.
[39] K. Jonnalagadda, N. Karanjgaokar, I. Chasiotis, J. Chee, D. Peroulis, Acta Mater. 58 (2010) 4674–4684.
[40] X.Y. Li, Y.J. Wei, W. Yang, H.J. Gao, Proc. Natl. Acad. Sci. USA 106 (2009) 16108–16113.
[41] T.H. Courtney, Mechanical Behavior of Materials, second ed., McGraw Hill, USA, 2000.
[42] F. Wu, H.M. Wen, E.J. Lavernia, J. Narayan, Y.T. Zhu, Mater. Sci. Eng. A 585 (2013) 292–296.
[43] Y.B. Wang, X.Z. Liao, Y.H. Zhao, E.J. Lavernia, S.P. Ringer, Z. Horita, T.G. Langdon, Y.T. Zhu, Mater. Sci. Eng. A 527 (2010) 4959–4966.
[44] S. Ni, Y.B. Wang, X.Z. Liao, R.B. Figueiredo, H.Q. Li, S.P. Ringer, T.G. Langdon, Y. T. Zhu, Acta Mater. 60 (2012) 3181–3189.
[45] X.L. Wu, X.Z. Liao, S.G. Srinivasan, F. Zhou, E.J. Lavernia, R.Z. Valiev, Y.T. Zhu, Phys. Rev. Lett. 100 (2008) 95701.
[46] J. Wang, N. Li, O. Anderoglu, X. Zhang, A. Misra, J.Y. Huang, J.P. Hirth, Acta Mater. 58 (2010) 2262–2270.
[47] X.L. Wu, Y.T. Zhu, Phys. Rev. Lett. 101 (2008) 25503.
[48] J.G. Brons, H.A. Padilla, G.B. Thompson, B.L. Boyce, Scr. Mater. 68 (2013) 781–784.
[49] Y.M. Wang, F. Sansoz, T. LaGrange, R.T. Ott, J. Marian, T.W. Barbee, A.V. Hamza, Nat. Mater. 12 (2013) 697–702.
[50] Y. Liu, J. Jian, Y. Chen, H. Wang, X. Zhang, Appl. Phys. Lett. 104 (2014) 231910.